International Journal of Engineering and Advanced Technology (IJEAT)
ISSN: 2249-8958 (Online), Volume-2 Issue-3, February 2013

Transformer less Soft Switching Bidirectional DC-DC Chopper

Baburaja.C, J.Jayakumar

Abstract*— Transformer less Soft Switching Bidirectional DC-DC Chopper has been proposed in this paper. The above mentioned system can be operated with ZVS, fixed switching frequency, and a ripple-free inductor current regardless of the power flow direction. To provide ZVS of the power switches and a ripple-free inductor current, the proposed converter utilizes a simple auxiliary circuit that consists of an additional winding to the main inductor and an auxiliary inductor. In the ZVS operation, the reverse recovery problem of the anti parallel body diode of the power switch does not occur. The ripple-free inductor current can reduce the voltage ripple. Analysis of the proposed bidirectional DC-DC converter a discussed in detail, and the experimental results obtained on 100-W prototype are analyzed in this paper.

Index Terms*—Bidirectional DC-DC converter, DC-DC power conversion ,zero-voltage-switching.

I. INTRODUCTION

Bidirectional DC-DC converters have been widely used in various industrial applications such as renewable energy systems, fuel cell vehicle, hybrid electric vehicle and uninterruptible power supplies. In those applications, bidirectional DC-DC converters control the power flow between the dc bus and the low-voltage sources such as back-up batteries, fuel cells, and super capacitors. Bidirectional DC-DC converters can be classified into isolated versions [3]–[8] and nonisolated versions [9]–[16]. It depends on the application.

This paper focuses on the transformer less Soft Switching Bidirectional Dc-DC Chopper . This converter is based on a half-bridge configuration where the combination of boost and buck converter.The conventional nonisolated bidirectional DC-DC converter is shown in Fig. 1. Both boost and buck modes, the conventional bidirectional DC-DC converter can operate in continuous conduction mode (CCM).

Although the CCM operation can provide a low ripple current ,switching loss of the power switches is large and there exists the reverse recovery phenomenon of the anti parallel body diode of the power switch. With a smaller inductance, the conventional converter can operate with an inductor current that flows in both directions during each switching period.

Manuscript published on 28 February 2013.
***** Correspondence Author (s)
Baburaja.C, Dept. Electrical and Electronics Engg/Karunya university/Coimbatore/India.
Dr.J.Jayakumar., Dept. Electrical and Electronics Engg/karunya university/Coimbatore/India.

Thus ZVS operation of the power switches is achieved. However, large inductor current ripple causes large voltage ripple and shortens lifetime of low-voltage sources such as batteries and fuel cells. Interleaving technique can be chosen to the bidirectional DC– DC converters. If there are several identical bidirectional ZVS DC-DC converters connected in parallel, current ripple problem can be solved [10]–[12]. However, the multichannel interleaved structure has many components and its control algorithm is complex.

Since the conventional non isolated bidirectional DC-DC converter shown in Fig.1 provides a continuous inductor current, the auxiliary circuits providing ZVS function can be a solution [9], [14]. However, most of them include one or more active switches which raise the overall cost. In order to remedy these problems, a new non isolated bidirectional ZVS DC-DC converter is proposed. This proposed converter can be operate as ZVS, fixed switching frequency, and a ripple free inductor current regardless of the direction of power flow.

A simple auxiliary circuit that consists of an additional winding to the main inductor and an auxiliary inductor provides ZVS function and cancels out the ripple component of the inductor current. The ripple-free inductor current can enlarge the lifetime of the battery that is usually used as a low side voltage source. The theoretical analysis is provided in the following section. The theoretical analysis is verified by a 100-W experimental prototype.

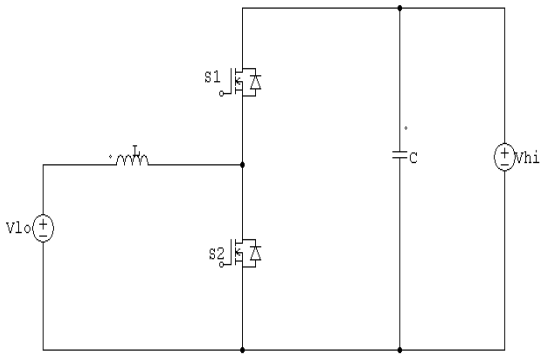

Fig.1 Conventional Bidirectional DC-DC Converter.

II. ANALYSIS OF THE PROPOSED CONVERTER

Fig. 1 shows a conventional nonisolated bidirectional DC-DC converter. In boost mode, the switch *S*2 acts as a boost switch and the switch *S*1 acts as a boost diode.

Published By:
Blue Eyes Intelligence Engineering and Sciences Publication (BEIESP)

In buck mode, *S*1 acts as a buck switch and *S*2 acts as a buck diode. Typically, back-up batteries or super capacitors act as the low side voltage source *V*lo . The dc voltage bus as the high side voltage source *V*hi. The capacitor *Cf* represents the high-frequency filter capacitor at dc bus. The proposed bidirectional DC-DC converter is shown in Fig. 2. It is very similar to the conventional converter except that an additional winding *Ns* to the main inductor and auxiliary inductor *Ls* are added and the filter capacitor *Cf* is split into *Cf* 1 and *Cf* 2. This auxiliary circuit provides ZVS function and cancels out the ripple component of the main inductor current regardless of the direction of power flow. The equivalent circuit of the proposed converter is shown in Fig. 3.

The coupled inductor *Lc* is modeled as a magnetizing inductance *Lm* and an ideal transformer that has a turn ratio of Np*: Ns* (= 1: *n*). The leakage inductance of the coupled inductor *Lc* is included in the auxiliary inductor *Ls.* The diodes *D*1 and *D*2 represent the intrinsic body diodes of *S*1 and *S*2. The capacitors *C*1 and *C*2 are the parasitic output capacitances of *S*1 and *S*2. Since the capacitances of capacitors *Cf* 1 and *Cf* 2 are large enough, they can be considered as voltage sources *VCf* 1 and *VCf*2 during a switching period. The average of the voltage across the inductor should be zero at steady-state according to volt-second balance law, the average values of the filter capacitors voltages *VCf* 1 and *VCf* 2 are equal to the voltages *V*hi−*V*lo and *V*lo, respectively. Fig. 4(a) shows the theoretical waveforms for the boost mode of the proposed converter. Fig. 4(b) describes the buck mode of the proposed converter. Fig. 5 shows the operating modes of boost and buck modes. Both boost and buck modes have four operating modes during a switching period *Ts* (= *t*4−*t*0).

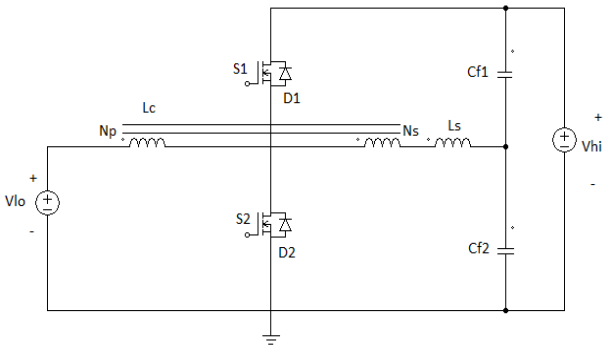

Fig.2 Circuit Diagram of the Proposed Bidirectional DC-DC Converter.

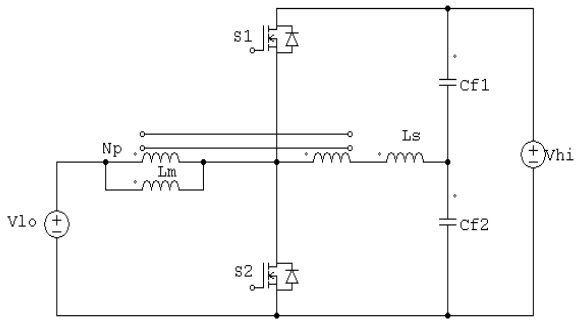

Fig.3 Equivalent Circuit of the Proposed Converter

A. Boost Operation

As shown in Fig. 4(a), before *t*0, *S*1 is conducting. The magnetizing current *im* decreases linearly and the current *iLs* increases linearly. At *t*0, they have their minimum and maximum values *Im*2 and *ILs*1, respectively. *Mode 1 [t*0, *t*1*]:* This begins with turn-off of *S*1. The switch current *iS* 1 is (1−*n*)*ILs*1−*Im*2 at *t*0 .With an assumption that the capacitors *C*1 and *C*2 are very small and the time interval in this mode is very short, so that all the currents can be considered as constant and the voltages v_{S1} and v_{S2} vary linearly. The transition time interval *Tt* 1 can be simplified as follows:

$$T_{t1} = \frac{(C_1+C_2)V_{hi}}{(1-n)I_{Ls1}-I_{m2}} \quad (1)$$

*Mode 2 [t*1, *t*2 *]:* At *t*1 , the voltage V_{S2} arrives at zero and the body diode D_2 of S_2 starts to conduct. Then, the gate pulse for the switch S_2 is applied. Since the voltage $V_{S\,2}$ is maintained as zero at the moment of the turn-on of S_2 , zero-voltage turn-on of S_2 is achieved. Since the voltage *vp* across the magnetizing inductance *Lm* is *V*lo , the magnetizing current *im* increases linearly from *Im*2 as follows

$$i_m(t) = I_{m2} + \frac{V_{lo}}{L_m}t \quad (2)$$

Since the secondary voltage *vs* across the secondary winding of the coupled inductor *Lc* is *nV*lo , the voltage *vLs* across the auxiliary inductor *Ls* is −(*1*−*n*)*V*lo . Then, the inductor current *iLs* decreases linearly as follows:

$$i_{Ls}(t) = I_{Ls1} - \frac{(1-n)V_{lo}}{L_s}t \quad (3)$$

Since the primary current *ip* is equal to *niLs*, the current at the low-voltage side *i*lo can be derived from (2) and (3) as follows:

$$i_{lo} = i_m(t) + i_p(t) = I_{m2} + nI_{Ls1} + \frac{V_{lo}}{L_m}t - \frac{n(1-n)}{L_s}V_{lo}t \quad (4)$$

Since the switch current *iS*2 is *i*lo−*iLs*, it can be obtained from (3) and (4). At the end of this mode, the inductor current *iLs* arrives at its minimum value −*ILs*2 and the magnetizing current *im* arrives at its maximum values *Im*1. *Mode 3 [t*2, *t*3 *]:* This mode begins with the turn-off of *S*2 .At this moment, the switch current *iS* 2 is *Im*1+(1−*n*)*ILs*2. This current starts to charge *C*2 and discharge *C*1. Similar to Mode 1, the transition time interval *Tt* 2 can be considered as follows:

$$T_{t2} = \frac{(C_1+C_2)V_{hi}}{(1-n)I_{Ls2}+I_{m1}} \quad (5)$$

*Mode 4 [t*3, *t*4 *]:* At *t*3 , the voltage *vS* 1 across the switch s1 arrives at zero and its body diode *D*1 starts to conduct. After that, the gate pulse for the switch *S*1 is applied. Since the voltage *vS* 1 is maintained as zero at the moment of the turn-on of *S*1 , zero voltage turn-on of *S*1 is achieved. In this mode, the voltage *vp* is −(*V*hi−*V*lo). Therefore, the magnetizing current *im* decreases linearly as follows:

$$i_m(t) = I_{m1} - \frac{V_{hi}-V_{lo}}{L_m} \quad (6)$$

Published By:
Blue Eyes Intelligence Engineering and Sciences Publication (BEIESP)

Since the voltage *vLs* across the inductor *Ls* is (1−*n*)(*V*hi −*V*lo), the current *iLs* increases linearly as follows:

$$i_{Ls}(t) = -I_{Ls2} - \frac{(1-n)V_{hi}-V_{lo}}{L_s}t \qquad (7)$$

From (6) and (7), the low-voltage side current *i*lo can be derived as follows:

$$i_{lo}(t) = I_{m1} - nI_{Ls2} - \frac{V_{hi}-V_{lo}}{L_m}t + \frac{n(1-n)V_{hi}-V_{lo}}{L_s}t \quad (8)$$

From (6) and (7), the low-voltage side current *i*lo can be derived as follows:

$$T_{t1} = \frac{(C_1+C_2)V_{hi}}{(1-n)I_{Ls1}+I_{m2}} \qquad (9)$$

Since the switch current *iS* 1 is *iLs*− *i*lo, it can be obtained from (7) and (8). At the end of this mode, the inductor current *iLs* arrives at its maximum value *ILs*1 and the current *im* arrives at its minimum values *Im*2.

B. Buck Operation:

The buck operation of the above proposed converter is identical to its boost operation except that the directions of the magnetizing current *im* and the low-voltage side current *i*lo are opposite to those in boot mode. As shown in Fig. 4(b), before *t*0, *S*1 is conducting. The magnetizing current *im* decreases linearly and the current *iLs* increases linearly.At *t*0, they have their minimumand maximum values −*Im*2 and *ILs*1, respectively. *Mode 1 [t*0, *t*1*]:* This begins with turn-off of *S*1. The switch current *iS* 1 is (1−*n*)*ILs*1+*Im*2 at *t*0 .With an assumption that the capacitors *C*1 and *C*2 are very small and the time interval in this mode is very short so that all the currents can be considered as constant and the voltages *vS* 1 and *vS*2 can consider to be vary linearly. The transition timeinterval *Tt* 1 can be simplified as follows:

$$i_m(t) = -I_{m2} + \frac{V_{lo}}{L_m}t \qquad (10)$$

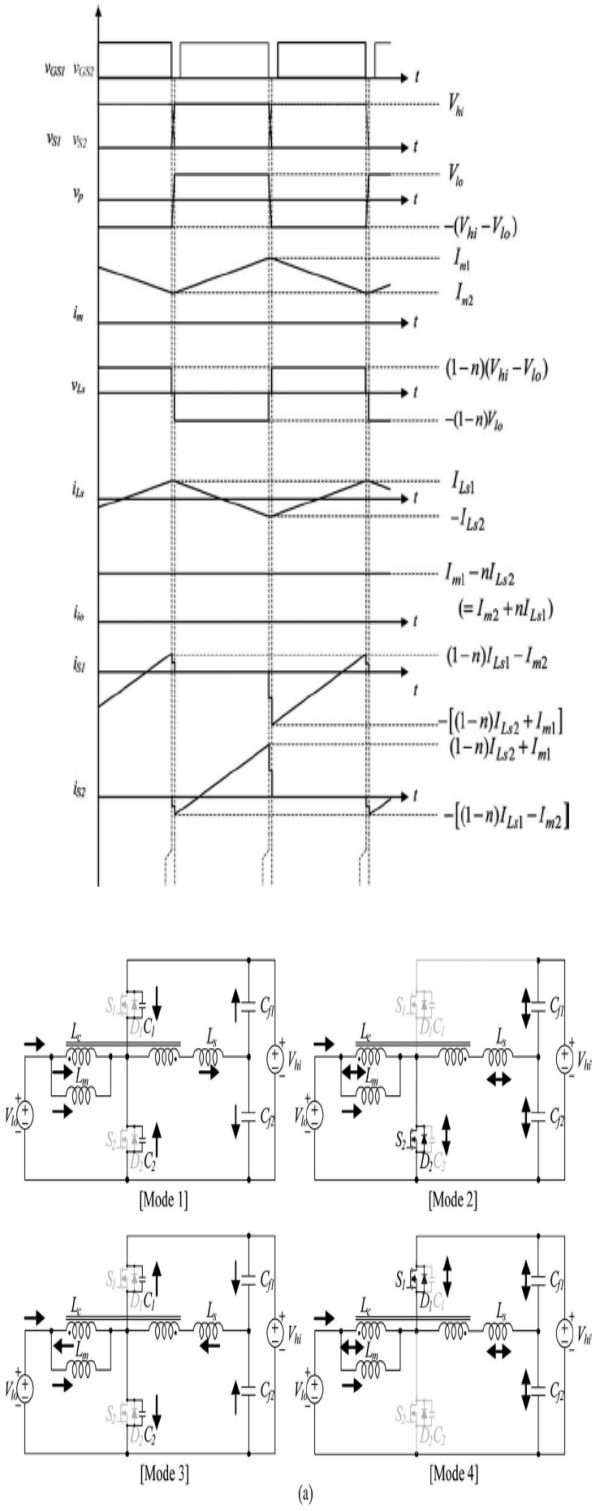

Fig.4 Operating Mode. (Boost mode).

*Mode 2 [t*1, *t*2*]:* At *t*1, the voltage *vS* 2 arrives at zero and the body diode *D*2 of *S*2 starts to conduct. Then, the gate pulse for the switch *S*2 is applied. Since the voltage *vS* 2 is maintained as zero at the moment of the turn-on of *S*2, zero-voltage turn-on of *S*2 is achieved. Since the voltage *vp* across the magnetizing inductance *Lm* is *V*lo , the magnetizing current *im* increases linearly from −*Im*2 as follows:

Published By:
Blue Eyes Intelligence Engineering
and Sciences Publication (BEIESP)

$$i_{Ls}(t) = I_{Ls1} - \frac{(1-n)V_{lo}}{L_s}t \quad (11)$$

Since the secondary voltage *vs* across the secondary winding of the coupled inductor *Lc* is *nV*lo , the voltage *vLs* across the auxiliary inductor *Ls* is $-(1-n)V$lo . Then, the inductor current *iLs* decreases linearly as follows

$$i_{lo}(t) = i_m(t) + i_p(t) = -I_{m2} + nI_{Ls1} + \frac{V_{lo}}{L_m}t - \frac{n(1-n)}{L_s}V_{lo}t \quad (12)$$

Since the primary current *ip* is equal to *niLs* and the low-voltage side current *i*lo can be derived from (10) and (11) as follows:

$$T_{t2} = \frac{(C_1+C_2)V_{hi}}{(1-n)I_{Ls2}-I_{m1}} \quad (13)$$

Since the switch current *iS* 2 is *i*lo−*iLs*, it can be obtained from (11) and (12). At the end of this mode, the inductor current *iLs* arrives at its minimum value −*ILs*2 and the magnetizing current *im* arrives at its maximum values −*Im*1 .*Mode 3 [t*2, *t*3 *]:* This mode begins with the turn-off of *S*2. At this moment, the switch current *iS* 2 is −*Im*1+ (1−*n*) *ILs2*. This current starts to charge *C*2 and discharge *C*1. Similar to Mode 1, the transition time interval *Tt* 2 can be considered as follows

$$i_m(t) = -I_{m1} - \frac{V_{hi}-V_{lo}}{L_m}t \quad (14)$$

*Mode 4 [t*3, *t*4]*:* At *t*3, the voltage *vS* 1 across the switch *S*1 arrives at zero and its body diode*D*1 starts to conduct. After that, the gate pulse for the switch *S*1 is applied. Since the voltage *vS* 1 is maintained as zero at the moment of the turn-on of *S*1, zero voltage turn-on of *S*1 is achieved. In this mode, the voltage *vp* is − (*V*hi−*V*lo). Therefore, the magnetizing current *im* decreases linearly as follows:

$$i_{Ls}(t) = -I_{Ls2} - \frac{(1-n)(V_{hi}-V_{lo})}{L_s}t \quad (15)$$

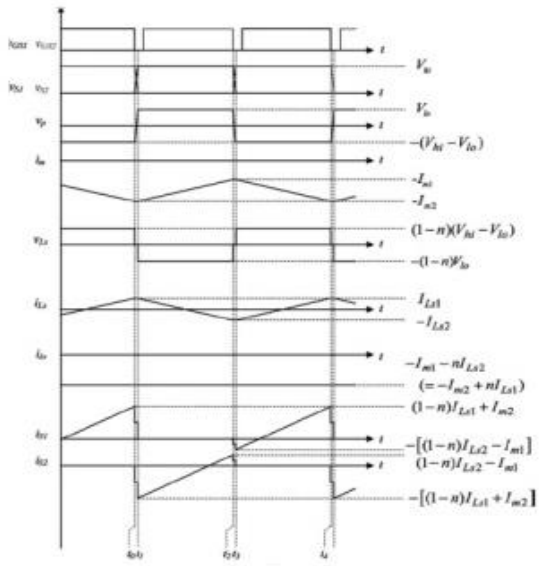

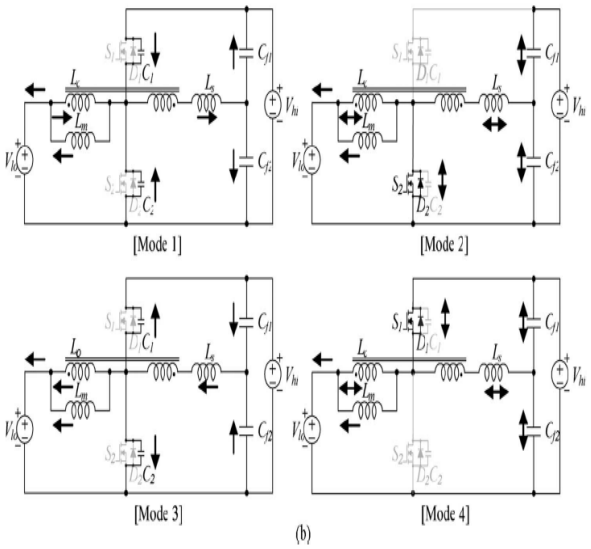

Fig.5.Operating Mode. (Buck mode)

Since the voltage *vLs* across the inductor *Ls* is (1−*n*)(*V*hi −*V*lo), the current *iLs* increases linearly as follows

$$i_{lo}(t) = -I_{m1} - nI_{Ls2} - \frac{V_{hi}-V_{lo}}{L_m}t + \frac{n(1-n)(V_{hi}-V_{lo})}{L_s}t \quad (16)$$

From (14) and (15), the low-voltage side current *i*lo can be derived as follows

$$L_s = n(1-n)L_m \quad (17)$$

Since the switch current i_{S1} is i_{Ls}− *i*lo , it can be obtained from (15) and (16). At the end of this mode, the inductor current i_{Ls} arrives at its maximum value I_{Ls1} and the current *im* arrives at its minimum values −*Im*2

C. Ripple Current Cancellation:

The ripple-free low-voltage side current can reduce the voltage ripple and enlarge the lifetime of the battery that is usually used as a low side voltage source. In the proposed converter, the ripple-free current characteristic can be easily achieved by utilizing the simple auxiliary circuit. From (4), (8), (12), and (16), the zero-ripple condition can be obtained by

$$V_{lo}DTs = (V_{hi} - V_{lo})(1-D)T_s \quad (18)$$

D. Relation between V_{lo} and Vhi

The relation between V_{lo} and V_{hi} is equal to that of the conventional bidirectional DC-DC converter shown in Fig. 1. Referring to the voltage waveforms *vp* across the magnetizing inductance *Lm* shown in Fig. 4(a) and 4(b), the volt-second balance law gives

$$\frac{V_{hi}}{V_{lo}} = \frac{1}{1-D} \quad (19)$$

Published By:
Blue Eyes Intelligence Engineering
and Sciences Publication (BEIESP)

Where $D=(t2-t1)/Ts$. Equation (18) can be rewritten as follows:

E. ILs1 and ILs2

The auxiliary inductor current *iLs* always flows through *Cf* 1 and *Cf* 2. Since the average value of a current flowing through a capacitor should be zero at steady state, it can be seen easily from Fig. 4(a) and (b) that *ILs*1 is equal to *ILs*2. From Modes 2 and 4 in both boost and buck modes, *ILs*1 and *ILs*2 can be obtained as follows:

$$I_{Ls1} = I_{Ls2} = \frac{(1-n)V_{lo}DTs}{2L_s} \quad (20)$$

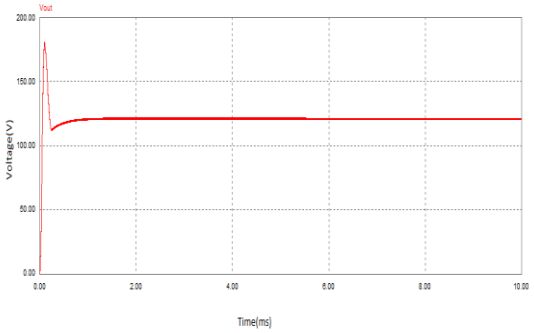

Fig.6 Boost Converter

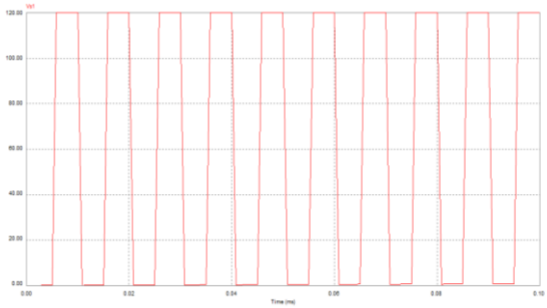

Fig.7 Pulse Across Switch S1

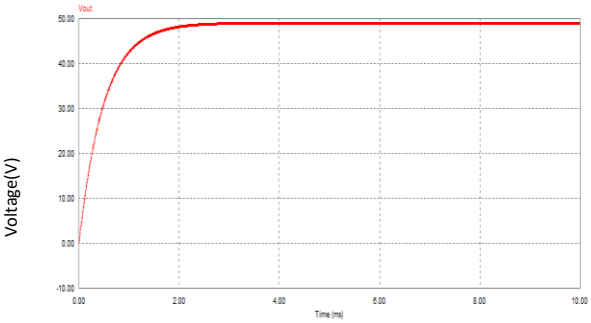

Fig.8 Buck Converter

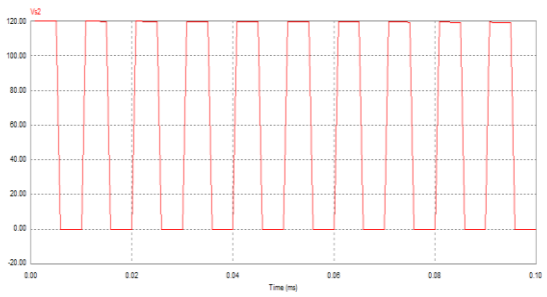

Fig.9 Pulse Across Switch S2

III. CONCLUSION

A new Transformer less Soft Switching Bidirectional Dc-DC Chopper has been proposed. ZVS of the power switches is always achieved and the reverse recovery problem of the anti parallel body diode of the power switches is solved in this work. Soft switching of power switches reduces the switching loss and improves the efficiency compared with the conventional non isolated bidirectional dc– dc converter when heavy load is applied. Moreover, it provides the ripple-free current characteristic in low-voltage side regardless of load condition. This characteristic of the above circuit can enlarge the lifetime of the low side voltage source.

REFERENCES

[1] H. Tao, J. L. Duarte, and M. A. M. Handrix, "Line-interactive UPS using a fuel cell as the primary source," *IEEE Trans. Ind. Electron.*, vol. 55, no. 8, pp. 3012–3021, Aug. 2008.

[2] L. R. Chen, N. Y. Chu, C. S. Wang, and R. H. Liang, "Design of a reflexbased bidirectional converter with the energy recovery function," *IEEE Trans. Ind. Electron.*, vol. 55, no. 8, pp. 3022–3029, Aug. 2008.

[3] F. Shang and Y. Yan, "Novel forward-flyback hybrid bidirectional DC-DC converter," *IEEE Trans. Ind. Electron.*, vol. 56, no. 5, pp. 1578–1584, May 2009.

[4] T.-F. Wu,Y.-C. Chen, J.-G. Yang, and C.-L. Kuo, "Isolated bidirectional full-bridge DC-DC converter with a flyback snubber," *IEEE Trans. Power Electron.*, vol. 25, no. 7, pp. 1915–1922, Jul. 2010.

[5] R.-J.Wai, C.-Y. Lin, andY.-R. Chang, "High step-up bidirectional isolated converter with two input power sources," *IEEE Trans. Ind. Electron.*, vol. 56, no. 7, pp. 2629–2643, Jul. 2009.

[6] H.Krishnsawami and N. Mohan, "Three-port series-resonant DC-DC converter to interface renewable energy sources with bidirectional load and energy storage ports," *IEEE Trans. Power Electron.*, vol. 24, no. 10, pp. 2289–2297, Oct. 2009.

[7] A. L. Kirsten, T. B. Marchesan, M. A. D. Costa, and R. N. do Prado, "Resonant technique for bidirectional flyback converter," *IET Electron.Lett.*, vol. 45, no. 25, pp. 1345–1346, Dec. 2009.

[8] H. Kim, C. Yoon, and S. Choi, "An improved current-fed ZVS isolated boost converter for fuel cell applications," *IEEE Trans. Power Electron.*, vol. 25, no. 9, pp. 2357–2364, Sep. 2010.

[9] P. Das, S. A. Mousavi, and G. Moschopoulos, "Anaysis and design of a nonisolated bidirectional ZVS-PWM DC-DC converter with coupled inductor," *IEEE Trans. Power Electron.*, vol. 25, no. 10, pp. 2630–2641, Oct. 2010.

[10] T. Bhattacharya, V. S. Giri, K. Mathew, and L. Umanand, "Multiphase bidirectional flyback converter topology for hybrid electric vehicles," *IEEE Trans. Ind. Electron.*, vol. 56, no. 1, pp. 78–84, Jan. 2009.

[11] W. Yu, H. Qian, and J.-H. Lai, "Design of high-efficiency bidirectional DC-DC converter and high-precision efficiency measurement," *IEEE Trans. Power Electron.*, vol. 25, no. 3, pp. 650–658, Mar. 2010.

[12] J. Zhang, J.-S. Lai, R.-Y Kim, and W. Yu, "High-power density design of a soft-switching high-power bidirectional DC-DC converter," *IEEE Trans.Power Electron.*, vol. 22, no. 4, pp. 1145–1153, Jul. 2007.

[13] L. Schuch, C. Rech, H. L. Hey, H. A. Grundling, H. Pinheiro, and J.R. Pinheiro, "Analysis and design of a new high-efficiency bidirectional integrated ZVT PWM converter for DC-bus and battery-bank interface," *IEEE Trans. Ind. Appl.*, vol. 42, no. 5, pp. 1321–1332, Sep. 2006.

[14] P. Das, B. Laan, S. A. Mousavi, and G. Moschopoulos, "A nonisolated bidirectionalZVS-PWMActive clampedDC-DC converter," *IEEE Power Electron.*, vol. 24, no. 2, pp. 553–558, Feb. 2009.

Published By:
Blue Eyes Intelligence Engineering and Sciences Publication (BEIESP)

[15] Y. Tsuruta, Y. Ito, and A. Kawamura, “Snubber-assisted zero-voltage and sero-current transition bilateral buck and boost chopper for EV drive application and test evaluation at 25 kW,” *IEEE Trans. Ind. Electron.*, vol. 56, no. 1, pp. 4–11, Jan. 2009.
[16] S. Dwari and L. Parsa, “An efficient high-step-up interleaved DC-DC converter with a common active clamp,” *IEEE Trans. Power Electron.*, vol. 26, no. 1, pp. 66–78, Jan. 2011.

Baburaja.C is pursuing his M.Tech degree in Power Electronics and Drives from Karunya University, Coimbatore, Tamilnadu, India. His research area includes Power Electronics, Energy Generation and Renewable Energy.

Dr.J.Jayakumar, is working as an associate Professor in Karunya University. He has 9 years of experience in teaching and 5 years in Research. His research area includes Power System Operation Modern Optimization Techniques

Published By:
Blue Eyes Intelligence Engineering and Sciences Publication (BEIESP)